Chapter-5

Temperature dependent drug delivery interaction and mechanical behaviour of SWCNT encapsulated Paclitaxel

Chapter 5. Temperature dependent drug delivery, interaction and mechanical behavior of SWCNT encapsulated Paclitaxel

5.1 Introduction

As one of the most common causes of death, cancer is a serious health problem globally with the mortality remaining constant. The common treatments for cancer include surgery, radiotherapy, chemotherapy, targeted therapy and immunotherapy, with chemotherapy being one of the most important treatments [1, 2]. Numerous chemotherapeutic drugs have been developed and used for the treatment of cancer, such as paclitaxel, cisplatin, 5-fluorouraci, cyclophosphamide, irinotecan, mitomycin C and doxorubicin [3–9]. However, the effectiveness of chemotherapy as compared to the immunotherapy is limited in cancer treatment due to low water solubility, lack of convincing anticancer activity, therapeutic selectivity and drug resistance especially multiple drug resistance (MDR) [10-13]. Therefore, the combination of various chemotherapeutic drugs with different mechanisms has become the standard clinical practice for cancer treatment [14-22].

Paclitaxel is a natural plant alkaloid that is isolated from the bark of the pacific yew tree and the active ingredient was firstly isolated and named as Taxol by Wani and Wall [23-25]. Paclitaxel (PTX) is a mitotic inhibitor for targeting tubulin by stabilizing the microtubule polymer and protecting it from disassembly to prevent the metaphase spindle configuration of chromosomes. This causes abnormality of mitotic spindle assembly, chromosome segregation, and cell division, resulting in blocking the progression of mitosis and prolonging activation of the mitotic checkpoint to trigger cell apoptosis or blocking cell cycle by arresting G2/M without cell division of treated cells [26-31].

Among all cancers, breast cancer is the most common cancer in women worldwide [32]. At present, paclitaxel is approved and widely used for the treatment of breast cancer in clinical conditions. PTX ($C_{47}H_{51}NO_{14}$) is a member of new class of anticancer agent that exerts its cytotoxic effect through a unique mechanism and it is poorly water-soluble. The challenge now days are to directly pass these macromolecules to cell membrane without any active

process. For this purpose, cremophore EL is used to make the drug soluble but, unfortunately cremophore EL itself is toxic. Hence, it is a prerequisite to find an alternative novel mechanism to introduce the bioactive molecule in the form of the drug delivery carrier in living cells [33, 34]. The potential drug delivery systems were found superior to free drugs (encapsulated drug) due to longer circulation time, higher drug uptake, selectively, lower dosage and better therapeutic efficiency [35]. Various studies have indicated that, the carbon nanotubes (CNTs) hold a great promise for effective delivery of biomolecules into cells [36, 37, 38] and cellular endoscope [39]. Moreover, CNTs have been used in several biomedical applications on account of their unique electrical, thermal and spectroscopic properties due to surface to volume ratio [40], CNTs have also been exploited as nanovectors for productive delivery of drugs and biomolecules by covalent and non-covalent attachment of biomolecules to its outer surface as well as inner surface by encapsulation. Number of studies have been reported which indicate that, the interaction between carbon-based materials and biomolecules can be the prime choice to conformational changes of biomolecules and also can control unwanted changes in biological functions [41, 42]. CNTs can be made biocompatible by chemical functionalization and functionalized CNTs can be biodegraded, which further authenticates their use as a carrier in physical environment (body environment). There are two types of CNTs, (1) Single walled carbon nanotube (SWCNT) and (2) multi walled carbon nanotube (MWCNT). SWCNT show the better binding affinity as compared to MWCNTs [43-47].

In the present work, we have encapsulated PTX in various chiral forms of SWCNTs such as, (12, 12), (13,13), and (15, 15) armchair to better understand their activity in the presence of body temperature and chemotherapeutic temperature in a physical environment. For this purpose molecular dynamics simulations (MDS) were implemented to study the time dependent behavior of the stated complex in the presence of water molecules [48] and body

environment such as pH and temperature. In a recent study, Rathod et al. have elaborated the relative role of PTX loaded and sialic acid functionalized MWCNT to target metastatic stage-dependent over-expression in colon cancer cells [49]. Water is the fluid that lubricates the working of the cells by attracting or rippling the water molecules, transporting the materials and molecular machinery and facilitating the chemical reactions. Dai et al. suggested a simple-walled CNT based drug delivery system for anticancer treatment by delivering of the doxorubicin (DOX, Adriamy cin, $C_{27}H_{29}NO_{11}$), a common drug used in chemotherapy (49-54). Wong and Xu [50] have investigated the interaction mechanism of DOX and SWCNT to understand the protonation and diameter effects on drug loading and releasing. They found that the adsorption on the side wall of CNTs and encapsulation in CNTs have distinct solvent, protonation and diameter dependency. Shaki et al. [51] modelled the interaction mechanism between anticancer drug penicillamine and pristine and functionalized CNTs and found that the functionalization of CNTs increases the drug adsorption. To interpret more precisely, here we evaluate the interaction and free energies between CNTs and PTX at various temperatures. We found that the encapsulation of PTX in (12, 12) and (13, 13) CNTs get damaged after the minimization (Figure 5.1). Therefore we continued the calculations with (15, 15) chirality having 20.53 Å diameter and 22.7 Å length.

5.2 Materials and Methodology

To study the interaction between PTX drug molecule and SWCNT, we considered three armchair chiralities of CNTs, (12, 12), (13, 13) and (15, 15). The drug adsorption behavior is evaluated by performing the MD Simulation (MDS). Finally, the armchair (15, 15) nanotube based on free energies and interaction mechanism which is consists of 540 carbon atoms is considered for further study. To understand the influence of the solvent effects on the adsorption behavior of PTX molecule, we performed the study in the presence of water molecules.

5.2.1 Simulation Specification

We have performed classical MD Simulations to elucidate the binding of PTX over SWCNT. Initial SWCNT has been modeled by the VMD-1.9.2 [52] while PTX encapsulated complex has been modeled by the UCSF chimera-1.11.2 [53]. The PTX topology was generated by the AnteChamber Python Parser interface (ACPYPE) [54]. To implement whole simulation GROMOS force field has been utilized [55]. Total 2606 TIP3P water molecules were added to each side of the 5nm dodecahedron simulation box. Once all topologies and complexes were developed the energy was brought to minimized state without constraints using steepest descent integrator for 500000 steps with the initial step size of 0.001 Å and minimization tolerance of 1500 kJ/(mol nm).

MD Simulations were performed on this energy-minimized system using the leap-frog algorithm under the NVT canonical ensemble. Hydrogen bond lengths were constrained which enable a time step of 0.5fs to be used for MD simulations [56]. Armchair SWCNT of n= 12, m=12 chirality with 20 Å length containing 432 carbon and 48 hydrogen, n= 13, m=13 chirality with 21 Å length containing 468 carbon and 52 hydrogen and n=15, m=15 chirality with 20.53 Å diameter, 22.7 Å length containing 540 carbon and 60 hydrogen atoms are considered. The nature of the interaction between CNT and organic molecules does not only depend on the organic molecule and CNT but also on the physical environment. Interaction and free energy behavior were observed for each of these conditions, thus enabling bond length constraints at 0.05 fs time step of simulations. The temperature coupling with v-rescale thermostat was implemented with time constant of 0.1 ps at a temperature of 315.15 K. No pressure coupling was applied to the system. Initial velocities were generated according to the Maxwell distribution at 300 K. The cutoff distance used for both the Coulombic and van der Waals interactions was 1.2 nm and the simulations were performed for 100ps. To control the

pressure, NPT ensemble simulation was performed for 10 ns and temperature coupling with v-rescale thermostat and pressure coupling with berendsen barostate [57] was applied for 0.1 and 2.0 time constant respectively. Temperature coupling was set at 310.15 K which is average body temperature. This temperature is also appropriate for the chemotherapy. All the simulations were performed using GROMACS MD simulation package at constant temperature (310.15 K & 315.15 K) and reference pressure (1 bar) [58].

5.2.2 Data Analysis

Root mean square deviation (RMSD) was calculated for the last frame of simulation. The atom-positional RMSD is most frequently used measure for structure comparison in structural biology. Its applications are diverse and include monitoring structural changes in simulations of protein folding and dynamics. [59, 60]

$$\text{RMSD (t1, t2)} = \sum_{Ni=1}^{N}(Xi(t2) - Xi(t1))1/2 \qquad (5.1)$$

X_i (t) is position of atom 'i' at time 't' and 'N' is the total number of atoms in the molecule. The first frame of trajectory (t1) is used as a reference and values of the RMSD were computed. The trajectories for each molecular system were analyzed to calculate the Lenard Jones (LJ) potential energy [61]. This was accomplished using the probability ratio method [62, 63]. The probability density distribution for the system was determined by first dividing the Surface Separation Distance (SSD) range of the simulation into 0.2 Å intervals (Δx_i). The probability density distributions were analyzed to calculate the overall interaction energy.

$$P_i = \frac{A_i}{\Delta xi} \quad with \sum(P_i \Delta x_i) = 1 \qquad (5.2)$$

Where, $'A_i'$ is positional probability.

Radial Distribution Function (RDF) helps to understand the interaction process in presence of micro-molecules. The increase in the intensity of RDF indicates more loosely packed

structure [64]. To describe the interatomic distance and interaction energy between molecules, we have used LJ potential as given by following equation.

$$V_{LJ} = \frac{A}{r^{12}} - \frac{B}{r^{6}} \quad (5.3)$$

Here, ‘r’ is the interatomic distance, ‘A’ and ‘B’ are repulsive and attractive LJ parameters, respectively which are calculated as a product of LJ parameters specific to atom types of the interacting particles [65]. MD simulations result were also validated using Solvent Accessible Surface Area (SASA), Radius of gyration (Rg), RDF, interaction energy and RMSD.

5.3 Results and Discussion

To understand the size and chirality dependent behavior of the considered SWCNT, we evaluated three distinct SWCNTs of fixed length (2.0 nm) and (12, 12), (13, 13), (15, 15) chiral geometries. All three geometries have been optimized by means of converging the total energy of the system using UCSF Chimera 1.11.2. We find that the encapsulation of PTX in (12,12) and (13,13) CNTs results in dissociation of surface hydrogen and carbon atoms of CNTs finally modulating the morphology and geometry of the CNTs (see Figure 5.1) [66]. Whereas, in case of the (15, 15) CNT, the PTX gets adsorbed inside the CNT without changing the geometry or morphology of the CNT (see Figure 2). The energy after optimizing the PTX encapsulated geometries of CNTs follows the trend $E_{(15,\ 15)} < E_{(13,\ 13)} < E_{(12,\ 12)}$ with magnitude -2.1728, -2.1655 and -2.0246 kJ/mol respectively. Thus we can conclude that, the (15, 15) CNT is the appropriate size of the CNT for encapsulating the PTX drug. This well-optimized structure has been considered for the assessment of the temperature dependent (310.15 K and 315.15 K) responses of the system.

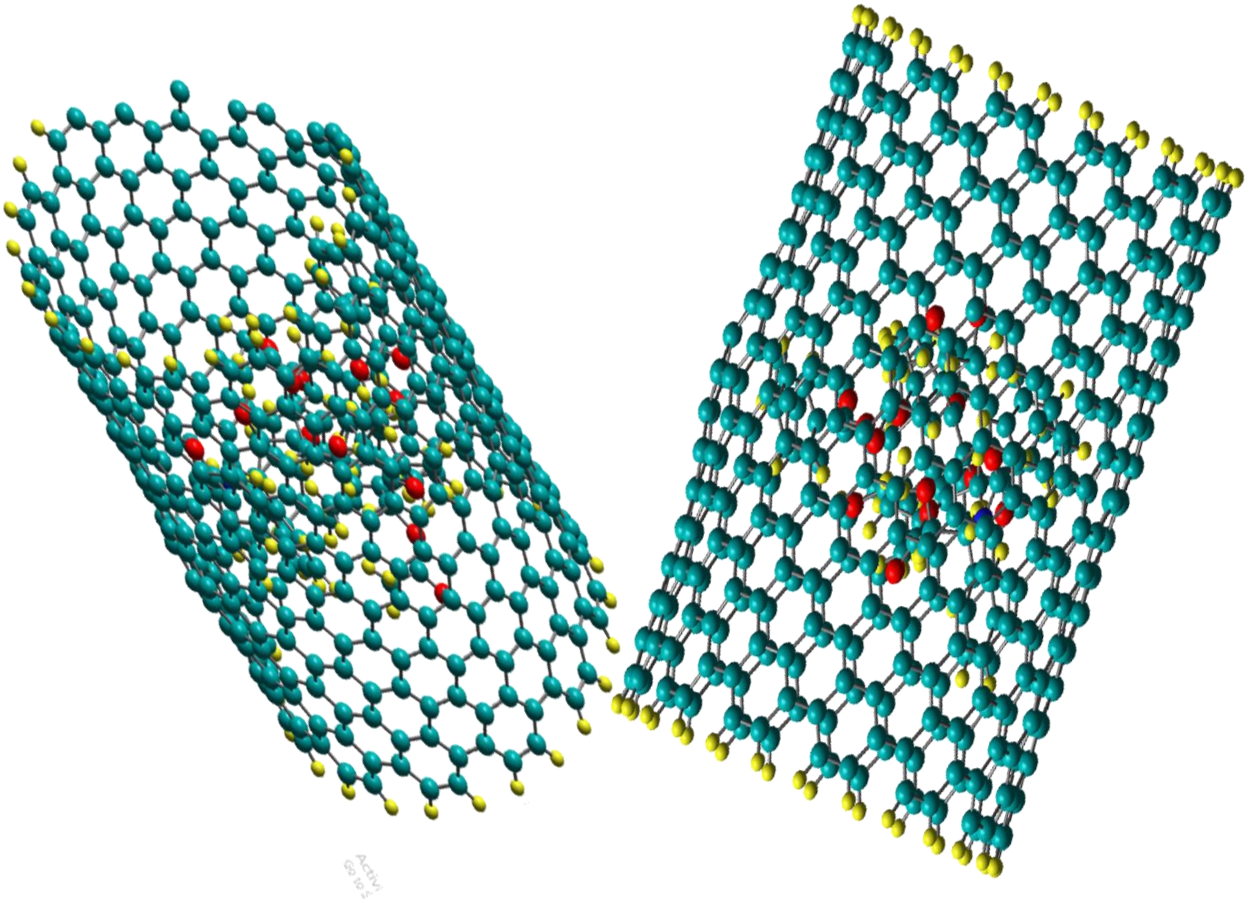

Figure 5.1. PTX encapsulated SWCNT with (a) n = 12, m = 12 and (b) n = 13, m = 13 chirality and length (L) = 2.0 nm.

Figures (Figure 5.2) specify the absorbance and delivery process with respect to time and temperature. Figure 5.2(a) carries the information regarding the interaction energy in the presence of 310.15 K and (b) 315.15 K temperature.

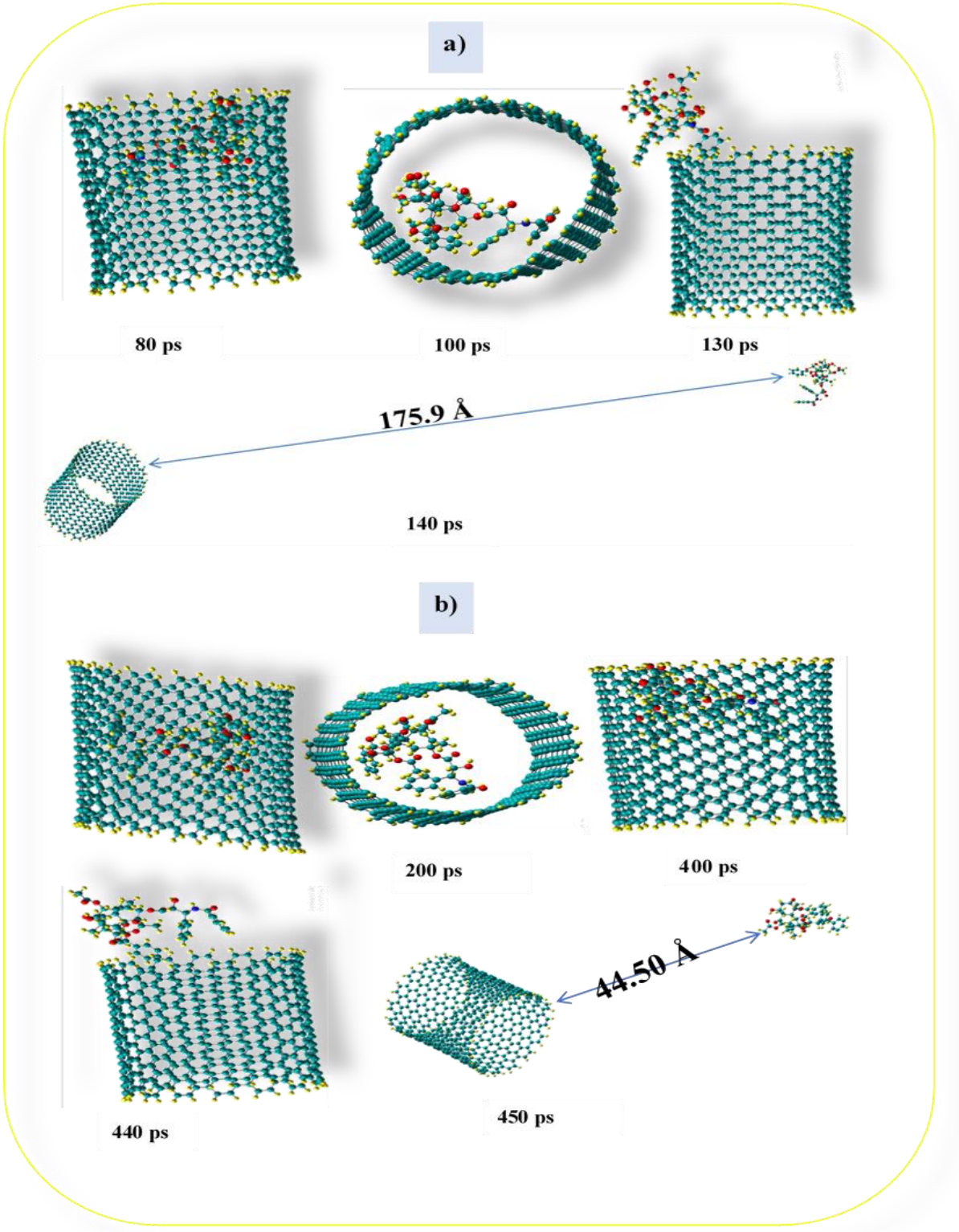

Figure 5.2: Time dependent snapshots of PTX encapsulated (15, 15) SWCNT with length (L) = 2.0 nm at temperatures (a) 310.15 K and (b) 315.15K.

These images were obtained at different timeslots to verify the exact drug delivery process. At 80ps under 310.15 K temperature, the drug is inside the delivery system while at 120 ps, the drug is getting outside and at 130 ps it is released from the carrier. Moreover, at 140 ps

the distance between the drug and carrier is 175.9 Å. Furthermore, at 315.15 K drug is getting outside after 430ps and released from the carrier at 440 ps. At 450 ps distance between them is 44.5 Å. As we know that the drug transport into a drug carrier can influence the drug release behavior from the carrier in the presence of the solvent. The solvent-controlled release includes osmosis-controlled release and swelling-controlled release [67]. From the above analyzed data we can say that, the drug is takes more time to release from the carriers with increase in the temperature. At chemotherapeutical (315.15 K) temperature, time required for the release is more than that at 310.15 K temperature; this implies we can control the process.

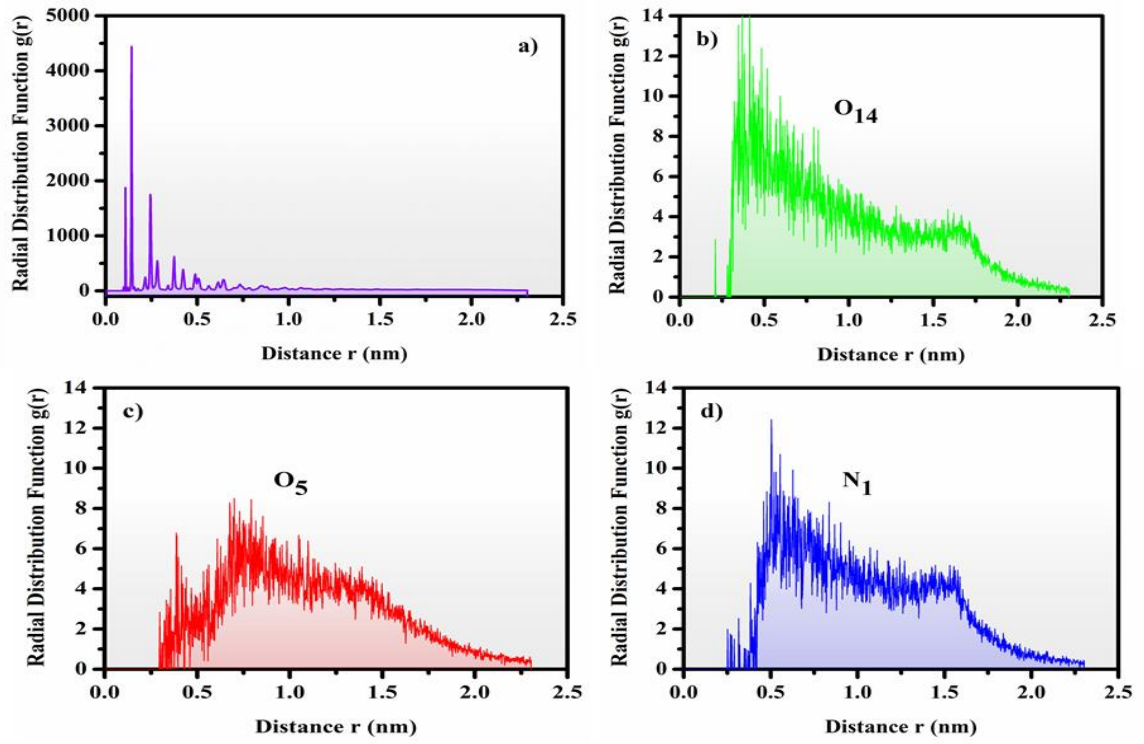

Figure 5.3: Computed radial distribution function of significant contributing atoms/molecule of PTX loaded SWCNT at temperature 310.15K: (a) PTX, (b) O_{14}, (c) O_5 and (d) N_1.

Figure 5.3 depicts the RDF per atom in the system. Figure 5.3(a) shows the RDF of PTX with respect to SWCNT. Range of 0 to 1nm have much higher amplitudes of PTX whereas, the $O_{14,}$ $O_{5,}$ and N_1 show high amplitudes between 0.2nm to 2.2nm with parabolic nature. These peaks are due to the inter-layer correlations in the PTX structure. Highest peaks for $O_{14,}$ $O_{5,}$

and N_1 are at r = 0.5, 0.7 and 0.6 respectively where, O_{14} carries the maximum radius of gyration 14.2g(r). Figure 5.3(b) shows the 315.15 K dependent RDF ratio, where, we can see that g(r) value is higher as compared to that at 310.15 K for the PTX structure Figure 5.4(a). Atoms $O_{14,}$ O_5 and N_1 exhibit high amplitude as compared to the body temperature structure (fig. 5.4 (a, b, c)) but after 1.5nm these peaks decrease. The sharp first few peaks confirm that the local correlations are well defined but additional disorder should be superimposed on the model. The present results suggest that the structures of the investigated atoms $O_{14,}$ O_5 and N_1 are related to the turbostratic one rather than to that of 310.15 structure.

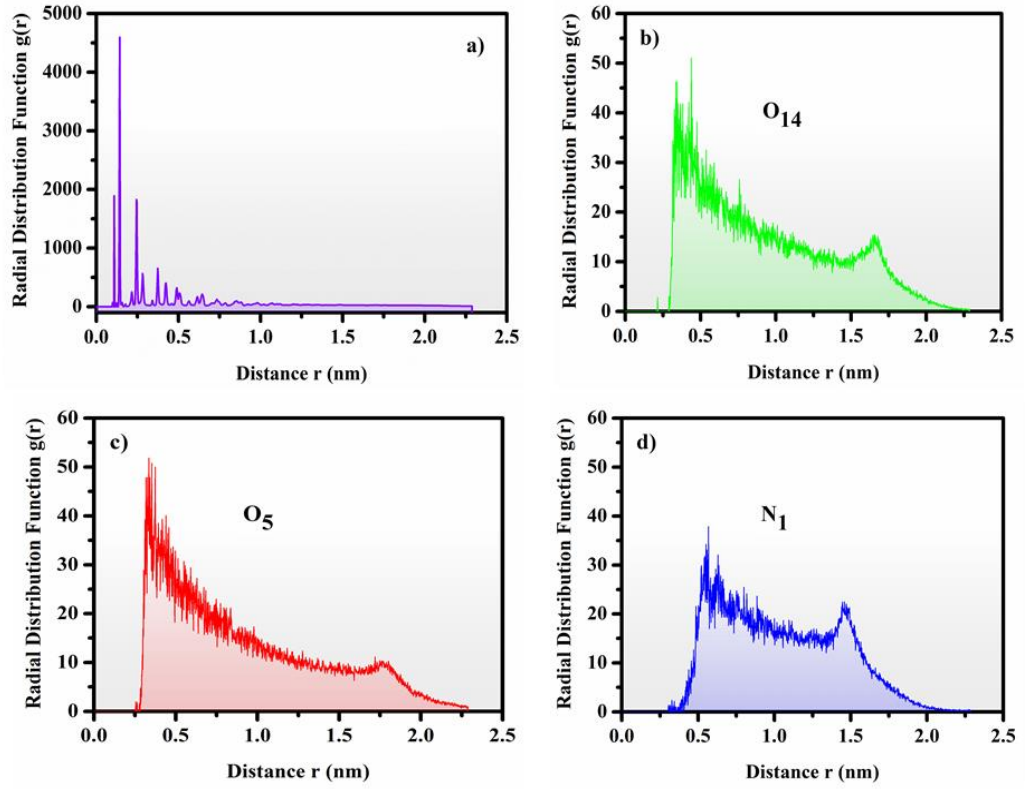

Figure 5.4: Computed radial distribution function of significant contributing atoms/molecule of PTX loaded SWCNT at temperature 315.15K: (a) PTX, (b) O_{14}, (c) O_5 and (d) N_1.

5.3.1 Interaction Energy

The binding energy and dislodge process of the ligand molecule using LJ potential has been investigated for getting insight into the drug loading and release mechanism. Integration of the thermodynamic functions is a computational technique for evaluating the interaction energy of the

complex systems. The MD simulations of PTX encapsulated SWCNT in the anion, cation, and aqueous solution demonstrate the faster removal of partial charges form the molecule. Specifically, the anion functional groups like, $–NH_2$ and –COOH, are able to form a hydrogen bond to the carboxylate group of another anion. Part of the internal energy due to the interaction is calculated as the time average of the sum of the interparticle interaction energies. Interaction energy of the complex at 310.15 K temperature (Figure 5.5 (a)) is observed to be less in magnitude than that of the elevated 315.15 K temperature (see Figure 5.5(b)). Comparing the trends of the interaction energy of the complex at both temperatures suggests higher magnitude of energy at elevated temperature indicating the stable configuration of the complex under temperature modification. At ~350 ps time, the computed interaction energy is -296.95 and -315.99 $kJ.mol^{-1}$ for 310.15 K and 315.15 K, respectively. Figure 5.5 (a) and (b) depict numerous small peaks before 350 ps time scale indicate feeble yet unavoidable interaction between the PTX and SWCNT. Interestingly, at 310.15 K after 110 ps and at 315.15 K after 440 ps the interaction energy follows quite different trend. A rapid dislodge process is observed; as illustrated in Figure 5.5(a), the PTX is observed to be still in alignment with the longitudinal axis of the SWCNT before 110 ps, however, after this, it rapidly moves out of the SWCNT (see Figure 5.5(a)). Similarly, in Figure 5.5(b) PTX takes 440ps to get released from the SWCNT. In addition, the system has approached agitation state at defined time with no modulation in the structural or morphological configurations.

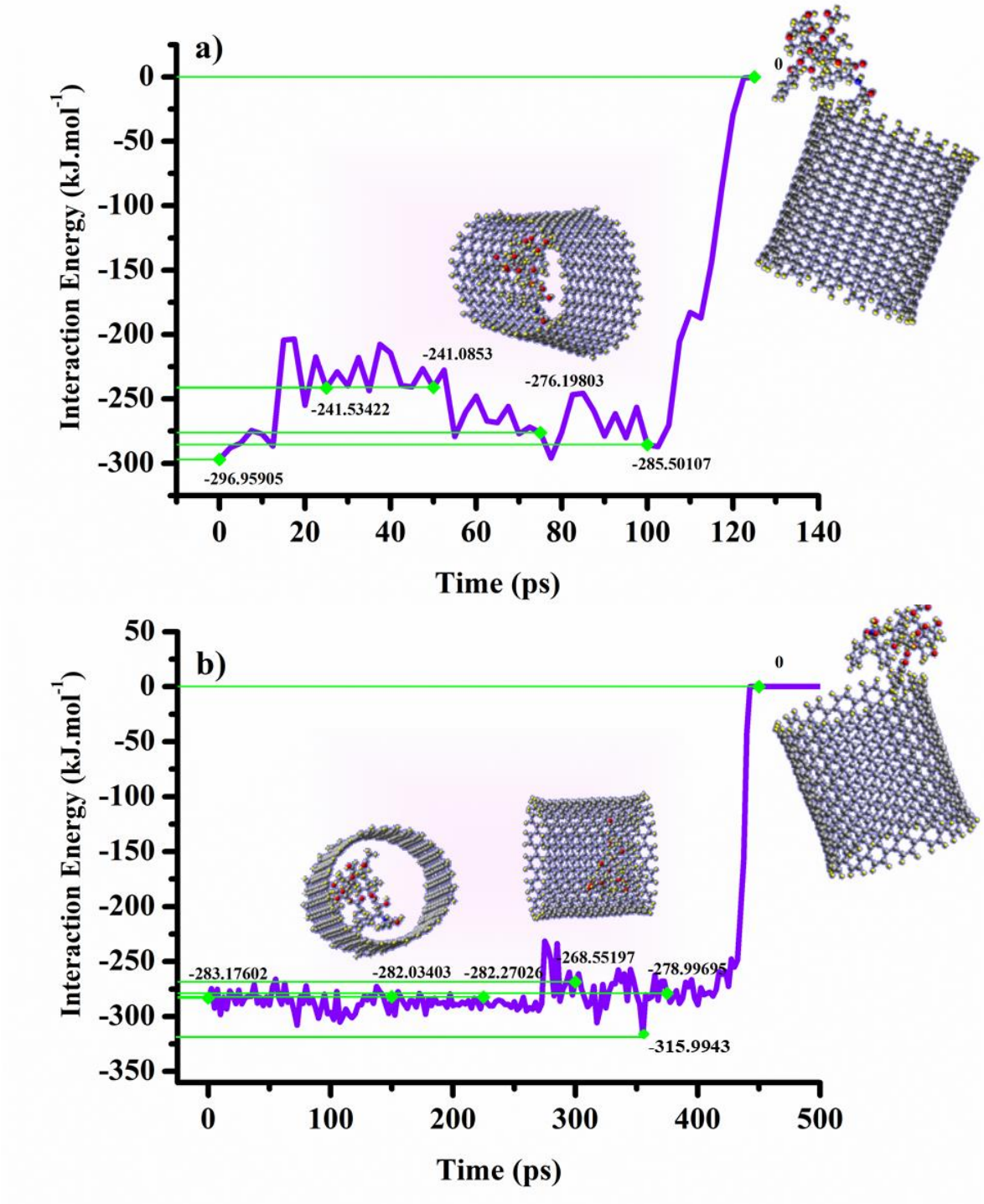

Figure 5.5: Temperature dependent interaction energy of the PTX encapsulated SWCNT as a function of time for temperatures (a) 310.15 K and (b) 315.15 K.

5.3.2 Solvation Accessible Area Analysis

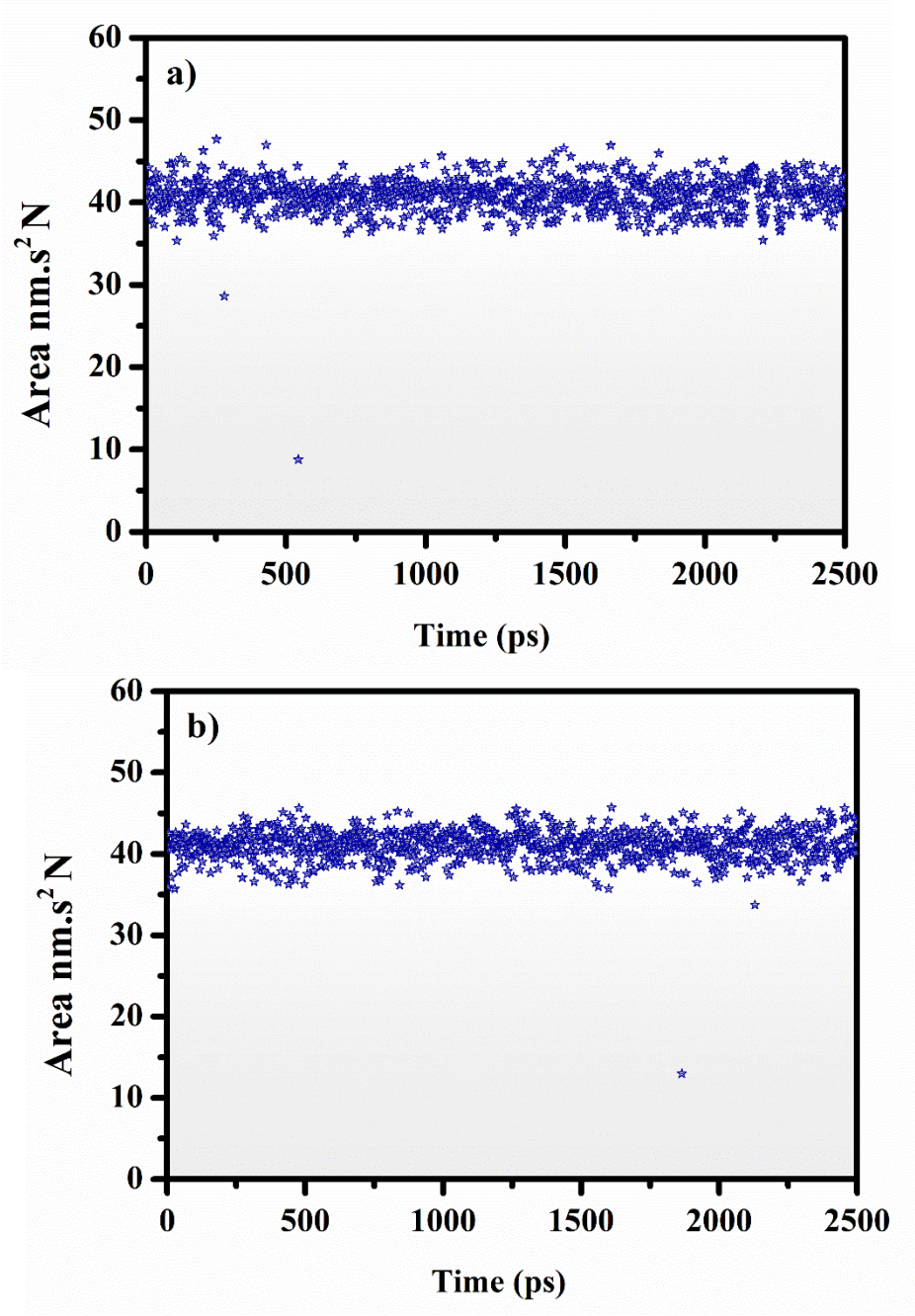

Figure 5.6. Calculated temperature dependent SASA as a function of time for temperatures (a) 310.15 K and (b) 315.15 K.

We proposed an approach of calculating conformational entropies using Solvent Accessible Surface Areas (SASA). SASA is an estimation of the surface of a molecule accessible to the solvent. The MD simulations have been utilized for calculating the SASA of the PTX encapsulated SWCNT at the considered temperatures (Figure 5.6). The average solvation energy has been calculated using the atomic solvation parameter 'Δσ' in a similar manner as that of

Wesson and Eisenberg [68]. The study of Wesson and Eisenberg [68] provided key insight to understand the role of a polymer in contact with the solvent. The physiochemical property, SASA as shown in the Figure 5.6 (a-b) remains almost constant with respect to time, except around 500 ps, where it shows gradual decrease at 310.15 K temperature. Similar trend is observed for 315.15 K temperature but at different time step of 1800 ps.

5.3.3 Radius of Gyration

The radius of gyration (R_g) is the root mean square distance of collection of masses from their center of gravity. This concept was introduced by Lagrange, who related the center of gravity for a system of masses to the distances between their centers. The radius of gyration of PTX encapsulated SWCNT is evaluated to measure its compactness at various temperatures. Increase in the temperature results in reduction of the end-to-end distance of the chain, thereby causing decrease in the radius. Further, the results indicate (see Figure 5.7) that the radius of gyration is maximum at 2250 ps . It is interesting to note that, the R_g remains almost constant for 310.15 K suggesting that, the R_g is unaffected by the complex formation. However, at elevated temperatures (Figure 5.7(b)) the R_g concentration is observed to be insignificant below time 400ps, with markable increase within the time range 400-1750ps followed by a sudden fall in the magnitude above 1750ps. This dramatic behavior of the R_g represents unusual nature and uncertainty which can be expected due to rise in temperature.

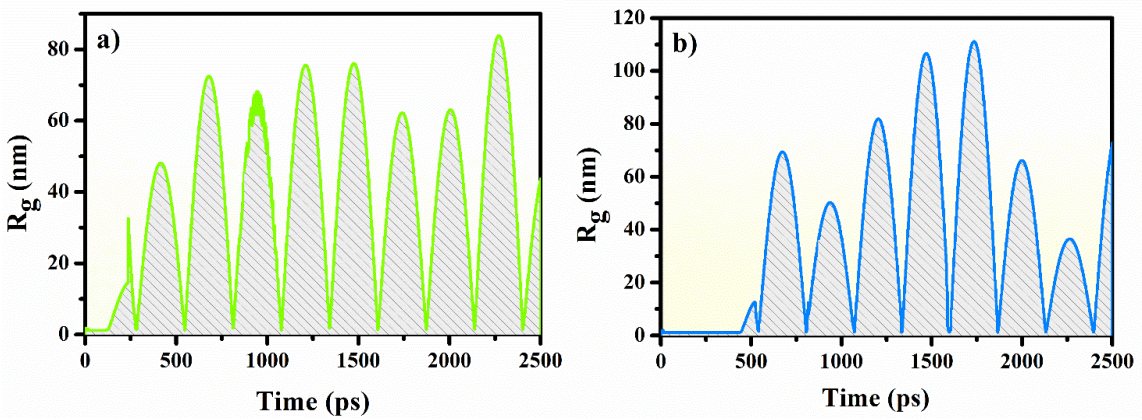

Figure 5.7: Computed radius of gyration of the system at temperatures a) 310.15K and b) 315.15K.

5.3.4 Root Mean Square Deviation (RMSD) Analysis

RMSD heavily depends on the precise superimposition of the two structures and is strongly affected by the most deviated fragments. The MD simulations give access to unravel the time and temperature dependent behaviour of the complex system. The modulation in the stability of the complex system can be investigated by performing the (RMSD) analysis. The structural stability is the fundamental property responsible for enhancing the biomolecular function, activity and regulation. The stability analysis of PTX encapsulated SWCNT complex (Figure 5.8) infers that the complex at both temperatures possess similar nature throughout the simulation. Higher stability also increases the rigidity and decreases stability which implies improved flexibility of structure. Conformational changes are also required for the structure to perform its normal functions, but the conformational flexibility and rigidity must be finally balanced. Hence, a high flexibility of complex due to incorporation of PTX at 315.15K temperature is observed.

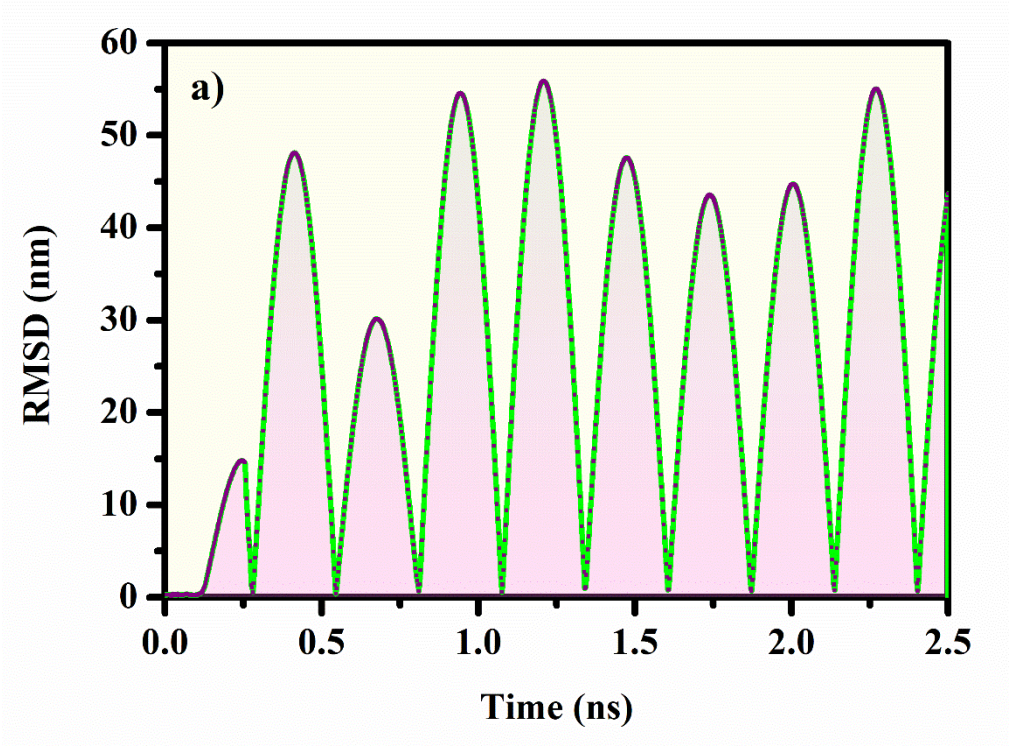

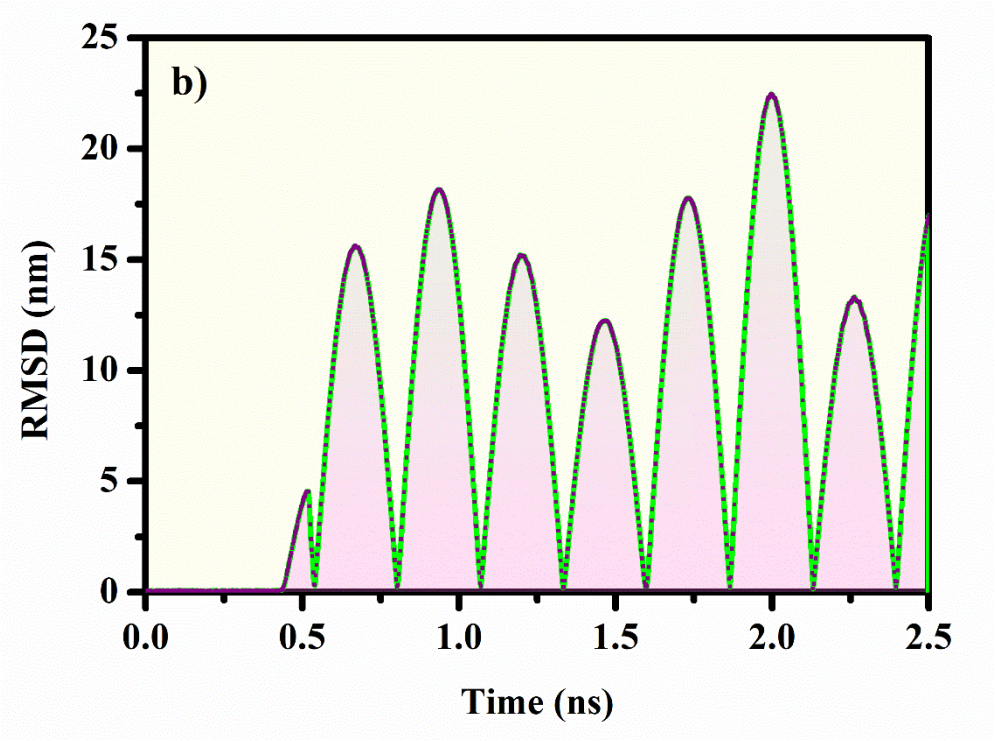

***Figure 5.8:** Temperature dependent root mean square deviation (RMSD) of PTX encapsulated SWCNT at temperatures (a) 310.15K and (b) 315.15K.*

5.4 Conclusion

In silico investigation of anti-cancer drug paclitaxel (PTX) loading within three different armchair SWCNTs with chirality (12, 12), (13, 13) and (15, 15) is performed. The systematic classical mechanics-based MD simulations of PTX encapsulation within the considered SWCNTs suggests that the SWCNT with (15, 15) chirality configuration is well-suited for PTX loading and delivery. Thus, a thorough investigation of this well-suited (15, 15) SWCNT with diameter 22.7 Å is performed by including the interaction of the PTX drug along the sidewalls of the SWCNT, its encapsulation within the SWCNT and their dependencies on the protonation of the NH group of PTX. The higher pair distribution function per atom of the complex with markable interaction energy indicates strong interaction between SWCNT and PTX. Further, the encapsulation is observed to get stronger at 315.15 K temperature owing to the higher absolute magnitude of the interaction energy. This replicates that the O-H/C-H..π and C=O.....π bonding and 20.53 Å diameter are optimal for proper encapsulation of the PTX with drug delivery time of 440ps at chemotherapeutic temperature. This observation is in accordance with the computed radial distribution function and interaction energy profiles. At 310.10 K temperature the SWCNT takes longer time to deliver the drug to diseased as compared to the 315.15 K temperature. In nut-shell, a thorough time and temperature dependent *in silico* investigation of the PTX encapsulation within the SWCNT under physical and chemotherapeutic temperatures suggests that the binding between the PTX and SWCNT enhances at elevated temperature and the release of the drug molecule is observed at prolonged time thereby giving enough time to SWCNT to reach within the proximity of the diseased area. Further, to get insight to the drug loading-release mechanism under practical circumstances, the interaction of the complex should be investigated within the proximity of the targeted cell membrane.

References

[1] T. Szekeres and L. Novotny, Med. Princ. Pract. **11**, 117 (2002).

[2] E. S. Wu, T. Oduyebo, L. P. Cobb, D. Cholakian, X. Kong, A. N. Fader, K. L. Levinson, E. J. Tanner III, R. L. Stone, A. Piotrowski, and others, Gynecol. Oncol. **140**, 76 (2016).

[3] S. Sideris, F. Aoun, M. Zanaty, N. C. Martinez, S. Latifyan, A. Awada, and T. Gil, Mol. Clin. Oncol. **4**, 1063 (2016).

[4] S. Dilruba and G. V Kalayda, Cancer Chemother. Pharmacol. **77**, 1103 (2016).

[5] X. Pan, X. Zhang, H. Sun, J. Zhang, M. Yan, and H. Zhang, PLoS One **8**, e56679 (2013).

[6] A. Emadi, R. J. Jones, and R. A. Brodsky, Nat. Rev. Clin. Oncol. **6**, 638 (2009).

[7] U. Vanhoefer, A. Harstrick, W. Achterrath, S. Cao, S. Seeber, and Y. M. Rustum, J. Clin. Oncol. **19**, 1501 (2001).

[8] T. Xu, L. Qin, Z. Zhu, X. Wang, Y. Liu, Y. Fan, S. Zhong, X. Wang, X. Zhang, L. Xia, and others, Oncotarget **7**, 27445 (2016).

[9] Y. J. Bae, Y. Il Yoon, T.-J. Yoon, and H. J. Lee, Korean J. Radiol. **17**, 497 (2016).

[10] Q. Zhou, M. Ye, Y. Lu, H. Zhang, Q. Chen, S. Huang, and S. Su, PLoS One **10**, e0136694 (2015).

[11] Z. Wei, L. Liang, L. Junsong, C. Rui, C. Shuai, Q. Guanglin, H. Shicai, W. Zexing, W. Jin, C. Xiangming, and others, J. Exp. Clin. Cancer Res. **34**, 1 (2015).

[12] M. Talekar, Q. Ouyang, M. S. Goldberg, and M. M. Amiji, Mol. Cancer Ther. **14**, 1521 (2015).

[13] J. Kenicer, M. Spears, N. Lyttle, K. J. Taylor, L. Liao, C. A. Cunningham, M. Lambros, A. MacKay, C. Yao, J. Reis-Filho, and others, BMC Cancer **14**, 1 (2014).

[14] A. J. Muñoz Mart\'\in, P. Garc\'\ia Alfonso, A. B. Rupérez, and M. Mart\'\in Jiménez, Oncol. Lett. **12**, 727 (2016).

[15] S. Ebara, Y. Kobayashi, K. Sasaki, M. Araki, M. Sugimoto, K. Wada, K. Fujio, A. Takamoto, T. Watanabe, H. Yanai, and others, Acta Med. Okayama **70**, 223 (2016).

[16] B. Kalaghchi, R. Abdi, F. Amouzegar-Hashemi, E. Esmati, and A. Alikhasi, Asian Pacific J. Cancer Prev. **17**, 287 (2016).

[17] A. Yilmaz, E. Alp, H. I. Onen, and S. Menevse, Contemp. Oncol. **20**, 28 (2016).

[18] M. Trendowski, T. D. Christen, C. Acquafondata, and T. P. Fondy, BMC Cancer **15**, 632 (2015).

[19] R. Van Der Noll, S. Marchetti, N. Steeghs, J. H. Beijnen, M. W. J. Mergui-Roelvink, E. Harms, H. Rehorst, G. S. Sonke, and J. H. M. Schellens, Br. J. Cancer **113**, 396

(2015).

[20] L. Huang, S. Chen, W. Yang, B. Xu, T. Huang, H. Yang, H. Zheng, Y. Wang, E. Song, J. Zhang, and others, Oncotarget **6**, 18683 (2015).

[21] B. Xiao, X. Si, M. K. Han, E. Viennois, M. Zhang, and D. Merlin, J. Mater. Chem. B **3**, 7724 (2015).

[22] N. Tsuda, H. Watari, and K. Ushijima, Chinese J. Cancer Res. **28**, 241 (2016).

[23] C. L. Schwab, D. P. English, D. M. Roque, and A. D. Santin, Anticancer. Drugs **25**, 522 (2014).

[24] M. C. Wani and S. B. Horwitz, Anticancer. Drugs **25**, 482 (2014).

[25] B. A. Weaver, Mol. Biol. Cell **25**, 2677 (2014).

[26] D. Zhang, R. Yang, S. Wang, and Z. Dong, Drug Des. Devel. Ther. **8**, 279 (2014).

[27] S. Takashima, S. Kiyoto, M. Takahashi, F. Hara, K. Aogi, S. Ohsumi, R. Mukai, and Y. Fujita, Oncol. Lett. **9**, 1822 (2015).

[28] N.-C. Chen, C.-C. Chyau, Y.-J. Lee, H.-C. Tseng, and F.-P. Chou, Sci. Rep. **6**, 20417 (2016).

[29] Z.-F. Zhong, W. Tan, S.-P. Wang, W.-A. Qiang, and Y.-T. Wang, Sci. Rep. **5**, 16415 (2015).

[30] K. Liu, S. Cang, Y. Ma, and J. W. Chiao, Cancer Cell Int. **13**, 10 (2013).

[31] E. Takatori, T. Shoji, S. Kumagai, T. Sawai, A. Kurose, and T. Sugiyama, J. Ovarian Res. **5**, 16 (2012).

[32] R. L. Siegel, K. D. Miller, and A. Jemal, CA. Cancer J. Clin. **66**, 7 (2016).

[33] Y. Guo, E. Terazzi, R. Seemann, J. B. Fleury, and V. A. Baulin, Sci. Adv. **2**, e1600261 (2016).

[34] S. Pogodin, M. Werner, J.-U. Sommer, and V. A. Baulin, ACS Nano **6**, 10555 (2012).

[35] A. Bianco, K. Kostarelos, M. Prato, Curr opin chem eng, 9, 674 (2005).

[36] X. Chen, A. Kis, A. Zettl, and C. R. Bertozzi, Proc. Natl. Acad. Sci. **104**, 8218 (2007).

[37] C. Tan, P. Yu, Y. Hu, J. Chen, Y. Huang, Y. Cai, Z. Luo, B. Li, Q. Lu, L. Wang, Z. Liu, and H. Zhang, J. Am. Chem. Soc. **137**, 10430 (2015).

[38] B. Nandy, M. Santosh, and P. K. Maiti, J. Biosci. **37**, 457 (2012).

[39] R. Singhal, Z. Orynbayeva, R. V. K. Sundaram, J. J. Niu, S. Bhattacharyya, E. A. Vitol, M. G. Schrlau, E. S. Papazoglou, G. Friedman, and Y. Gogotsi, Nat. Nanotechnol. **6**, 57 (2011).

[40] Z. Chen, A. Zhang, X. Wang, J. Zhu, Y. Fan, H. Yu, and Z. Yang, J. Nanomater. **2017**, 13 (2017).

[41] X. Sun, Z. Feng, T. Hou, and Y. Li, ACS Appl. Mater. Interfaces **6**, 7153 (2014).

[42] F. Stillinger, Nature, 401, 850 (1999).

[43] Z. Liu, X. Sun, N. Nakayama-Ratchford, and H. Dai, ACS Nano **1**, 50 (2007).

[44] Z. Liu, A. C. Fan, K. Rakhra, S. Sherlock, A. Goodwin, X. Chen, Q. Yang, D. W. Felsher, and H. Dai, Angew. Chemie - Int. Ed. (2009).

[45] N. M. Dinan, F. Atyabi, M.-R. Rouini, M. Amini, A.-A. Golabchifar, and R. Dinarvand, Mater. Sci. Eng. C **39**, 47 (2014).

[46] S. Lv, Z. Tang, M. Li, J. Lin, W. Song, H. Liu, Y. Huang, Y. Zhang, and X. Chen, Biomaterials **35**, 6118 (2014).

[47] H. Xu, M. Fan, A. M. A. Elhissi, Z. Zhang, K.-W. Wan, W. Ahmed, D. A. Phoenix, and X. Sun, Nanomedicine **10**, 1247 (2015).

[48] P. Ball and F. H. Stillinger, Nature **401**, 850 (1999).

[49] V. Rathod, R. Tripathi, P. Joshi, P. K. Jha, P. Bahadur, and S. Tiwari, Aaps Pharmscitech **20**, 51 (2019).

[50] Y. Wang and Z. Xu, RSC Adv. **6**, 314 (2016).

[51] H. Shaki, H. Raissi, F. Mollania, and H. Hashemzadeh, J. Biomol. Struct. Dyn. **38**, 1322 (2019).

[52] W. Humphrey, A. Dalke, K. Schulten, and others, J. Mol. Graph. **14**, 33 (1996).

[53] E. F. Pettersen, T. D. Goddard, C. C. Huang, G. S. Couch, D. M. Greenblatt, E. C. Meng, and T. E. Ferrin, J. Comput. Chem. **25**, 1605 (2004).

[54] A. W. S. Da Silva and W. F. Vranken, BMC Res. Notes **5**, 367 (2012).

[55] N. Schmid, A. P. Eichenberger, A. Choutko, S. Riniker, M. Winger, A. E. Mark, and W. F. van Gunsteren, Eur. Biophys. J. **40**, 843 (2011).

[56] M. Karplus and J. A. McCammon, Nat. Struct. Biol. **9**, 646 (2002).

[57] J. Lee, X. Cheng, J. M. Swails, M. S. Yeom, P. K. Eastman, J. A. Lemkul, S. Wei, J. Buckner, J. C. Jeong, Y. Qi, and others, J. Chem. Theory Comput. **12**, 405 (2016).

[58] J. Lemkul, Living J. Comput. Mol. Sci. **1**, 5068 (2018).

[59] X. Daura, B. Jaun, D. Seebach, W. F. Van Gunsteren, and A. E. Mark, J. Mol. Biol. **280**, 925 (1998).

[60] X. Daura, W. F. van Gunsteren, and A. E. Mark, Proteins Struct. Funct. Bioinforma. **34**, 269 (1999).

[61] L. S. Tee, S. Gotoh, and W. E. Stewart, Ind. Eng. Chem. Fundam. **5**, 356 (1966).

[62] M. Mezei, Mol. Simul. **3**, 301 (1989).

[63] W. F. van Gunsteren , P. K. Weiner and A.J. Wilkinson, editors. *Computer simulation of biomolecular systems: theoretical and experimental applications*. Springer Science & Business Media; (2013).

[64] H. Kovacs, J. Kowalewski, and A. Laaksonen, J. Phys. Chem. **94**, 7378 (1990).

[65] W. F. van Gunsteren and H. J. C. Berendsen, Groningen Molecular Simulation (GROMOS) Library Manual, Biomos, Groningen, The Netherlands, 1-221 (1987)

[66] S. Y. Madani, N. Naderi, O. Dissanayake, A. Tan, and A. M. Seifalian, Int. J. Nanomedicine **6**, 2963 (2011).

[67] R. Langer and N. Peppas, J. Macromol. Sci. Macromol. Chem. Phys. **23**, 61 (1983).

[68] L. Wesson and D. Eisenberg, Protein Sci. **1**, 227 (1992).